NANO LETTERS

xxxx
Vol. 0, No. 0
A−E

Vibrational Response of Au–Ag Nanoboxes and Nanocages to Ultrafast Laser-Induced Heating

Hristina Petrova,[†] Chien-Hua Lin,[§] Min Hu,[‡] Jingyi Chen,[‡] Andrew R. Siekkinen,[‡] Younan Xia,[‡,||] John E. Sader,[§,⊥] and Gregory V. Hartland*[,†]

Department of Chemistry and Biochemistry, University of Notre Dame, Notre Dame, Indiana 46556-5670, Department of Chemistry, University of Washington, Seattle, Washington 98195-1700, and Department of Mathematics and Statistics, The University of Melbourne, Victoria, 3010, Australia

Received February 4, 2007; Revised Manuscript Received March 5, 2007

ABSTRACT

Time-resolved spectroscopy has been used to investigate the vibrational properties of hollow cubic nanoparticles: Au–Ag nanoboxes and nanocages. In these experiments, laser-induced heating was used to coherently excite the breathing vibrational modes of the particle. The vibrational periods scale with the edge length of the particle and the nanocages and nanoboxes showing equivalent responses despite a large difference in their morphology. The measured vibrational periods are compared to finite element calculations, where the particles are modeled as a hollow cube, with the principle crystal axes parallel to the sides of the cube. Very good agreement is obtained between the calculations and the experimental data, with the experimental frequencies being slightly lower than the calculated values (by ~7%). These results demonstrate the importance of accurately modeling the particles in order to interpret experimental data.

Advances in synthetic techniques have made it possible to produce high-quality samples of metal and semiconductor nanoparticles in a variety of different shapes such as rods,[1−3] triangles,[4,5] cubes and boxes,[6] and branched structures.[7,8] These particles have unique optical properties and are finding use in a variety of applications from molecular sensing[9] to biological labeling[10] and photothermal therapy.[11,12] For metal particles, the optical response is dominated by the surface plasmon resonance (SPR), which is a coherent oscillation of the conduction electrons across the particle surface.[13] Recent research has focused on understanding how the position and width of the SPR depends on the size and shape of the particles.[14] In this regard, single-particle spectroscopy has been particularly useful.[15,16] These experiments have shown, for example, how radiation damping,[15,17] electron-surface scattering,[17,18] and the "lightning-rod effect"[19] control the width of the plasmon resonance.

Time-resolved experiments also provide information about the properties of nanoparticles. For metals, transient absorption experiments conducted on a subpicosecond time scale give information about electron−electron[20] and electron−phonon coupling.[21] At longer time scales (tens to hundreds of picoseconds) transient absorption measurements give data about how energy relaxes from the particle to the environment.[22,23] This information is important to photothermal therapy, where laser-induced heating of nanoparticles is used to kill selected cells.[11,12] For high-quality samples, modulations due to coherently excited vibrational modes can also be observed in the transient absorption traces.[22] These modes are excited by the rapid lattice heating that accompanies the electron−phonon coupling process.[24,25] The vibrational frequencies depend on the size, shape, and elastic constants of the particles. Thus, the study of these modes can provide information about the elastic properties of nanoparticles.[25,26]

To obtain quantitative information from the vibrational spectroscopy experiments, an expression is needed that relates the measured frequencies to the particle dimensions and elastic constants. For spheres (both homogeneous and core−shell) and rods, analytic expressions are available for the important modes observed in the transient absorption experiments.[24−27] However, for other shapes, the vibrational modes must be calculated numerically.[28] In our recent study of cubic silver nanoparticles, we used finite element analysis to calculate the natural vibrational modes of the particle.[29] The specific modes excited by the pump laser were determined by modeling the initial strain created by laser-induced heating and decomposing the initial strain into a sum over the normal modes.[29,30] This analysis predicted that two main modes should be observed in our experiments: the breathing

* Corresponding author. E-mail: ghartlan@nd.edu.
[†] Department of Chemistry and Biochemistry, University of Notre Dame.
[‡] Department of Chemistry, University of Washington.
[§] Department of Mathematics and Statistics, The University of Melbourne.
[||] E-mail: xia@chem.washington.edu.
[⊥] E-mail: J.Sader@ms.unimelb.edu.au.

10.1021/nl0702766 CCC: $37.00
Published on Web 03/15/2007

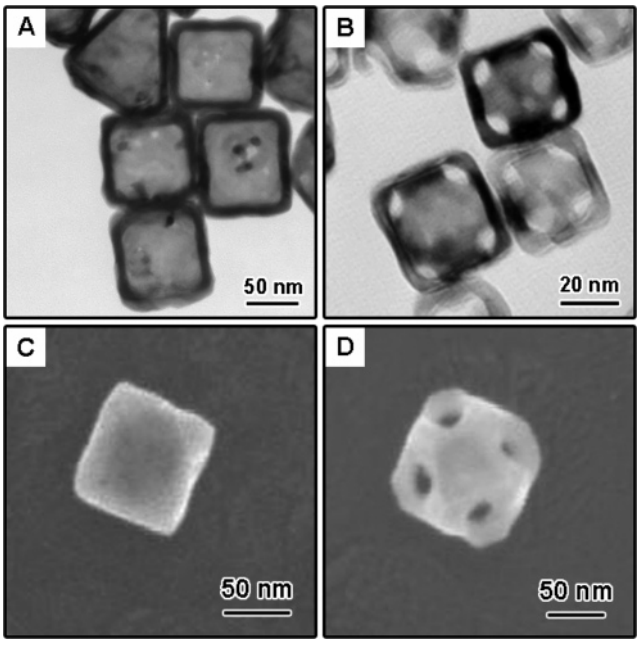

Figure 1. Representative TEM and SEM images of Au−Ag nanoboxes (left) and nanocages (right). The TEM images are shown on the top. Well-developed holes can be clearly seen on the nanocages but are not obvious on the nanoboxes.

mode of the cubes and a nontotally symmetric mode that arises from nonuniform heating effects (due to the finite penetration depth of the pump laser). The experimental and calculated frequencies were in reasonable agreement, revealing that the elastic constants of the particles are on the same level as bulk silver.

In this paper, we extend both the experiments and calculations to cubic particles with hollow interiors. These particles are made by a galvanic replacement reaction between Au(III) and silver nanocubes.[6] The particles are termed nanoboxes or nanocages, depending on whether small holes can be observed on the surface of the particle. Which type of particle is obtained is determined by the extent of the replacement reaction. A full description of the synthesis procedure is given in ref 31. Representative transmission electron microscopy (TEM) and scanning electron microscopy (SEM) images of the particles are shown in Figure 1. The nanoboxes are cubic with {100} facets.[6] In contrast, the nanocages have truncated corners, which give rise to additional {111} facets.[31] The holes in the nanocages typically develop on the {111} facets. Five different samples were studied: three nanobox samples and two nanocage samples. The average edge lengths and wall thicknesses for the different samples were measured by a combination of TEM and SEM measurements and are given in Table 1. The elemental composition of the samples was measured by atomic emission spectroscopy and was found to vary from a Au−Ag atomic ratio of 2:1 for the smaller particles (cage 1) to 3:1 for the larger particles (box 3).

Transient absorption experiments were performed using a regeneratively amplified Ti:sapphire laser system that has been described in detail elsewhere.[32] Pump pulse energies of approximately 2 μJ/pulse were used for the experiments,

Table 1. Average Dimensions (Edge Length L and Wall Thickness w), Measured Vibrational Periods, and the Corresponding Reduced Frequencies for the Five Different Samples[a]

sample	L (nm)	w (nm)	L/w	period (ps)	reduced frequencies
box 1	44.4 ± 4.1	5.7 ± 0.9	7.8 ± 2.0	45 ± 2	3.67 ± 0.18
box 2	58.2 ± 5.5	7.6 ± 1.2	7.6 ± 1.9	63 ± 2	3.44 ± 0.17
box 3	90.4 ± 7.1	9.8 ± 1.3	9.2 ± 1.9	93 ± 2	3.62 ± 0.18
cage 1	36 ± 4	4.4 ± 0.5	8.2 ± 1.8	39 ± 2	3.43 ± 0.17
cage 2	68 ± 12	7.2 ± 1	9.4 ± 3.0	72 ± 2	3.51 ± 0.18

[a] The errors correspond to the standard deviation.

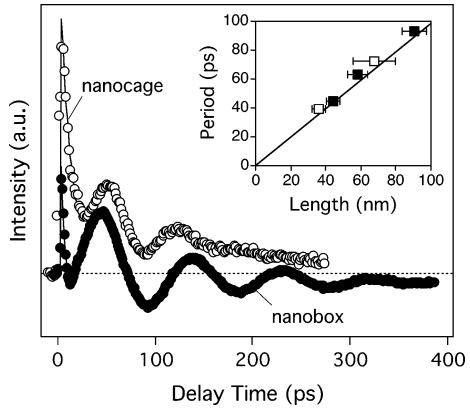

Figure 2. Transient absorption data for nanobox (box 3) and nanocage (cage 2) samples. The experiments were performed by exciting the samples with 400 nm pump pulses and probing in the near-IR spectral region (resonant to the SPR of the particles). The inset shows the measured vibrational periods plotted vs the edge length of the particles. The line is the calculated period (see text for details).

with a laser spot size at the sample of 2−4 mm^2. The pump laser wavelength was 400 nm, and the probe wavelengths used were 740, 750, 840, and 850 nm. These wavelengths span the SPR of the samples. Figure 2 shows typical transient absorption traces for a nanobox and a nanocage sample. The two traces show similar features: a fast decay at early times corresponding to the electron−phonon coupling process and a pronounced modulation due to the coherently excited vibrational modes.[24,25] The period of the vibrational modulation was obtained by fitting the data to a damped cosine term (solid lines in Figure 2). The average periods for the different samples, from all the probe wavelengths used, are collected in Table 1. Note that the decay times for the modulations are very different for the two samples in Figure 2. This is attributed to differences in the polydispersity: samples with narrower size distributions have longer vibrational lifetimes.[22] The inset in Figure 2 shows a plot of the average period versus the average edge length for the different samples, the closed symbols represent the nanoboxes, and the open symbols represent the nanocages. The line is the period calculated using the theoretical results derived below. This plot shows that the vibrational periods scale identically with dimensions for the nanoboxes and nanocages despite their substantial morphology difference.

Following our recent study of silver cubes,[29] the particles were modeled as a hollow cubic box composed of a linearly elastic material with cubic crystal symmetry. The principle crystal axes were set parallel to the sides of the box, corresponding to a particle with {100} surfaces. The experimental observation that the vibrational periods for all the samples fall on the same line versus edge length, see Figure 2, justifies the use of this simple model for both the nanocages and nanoboxes. The pump laser pulse is assumed to uniformly heat the box. In our calculations, the reference state is taken as the final equilibrium state of the hot particle. Thus, the initial state of the box immediately following the pump pulse is a uniform strain. This initial strain coherently excites vibrational modes of the particle via a displacive mechanism.[22,25,29] The relative amplitude α_n of the different modes in the particle response is obtained by expressing the time-dependent displacement $\boldsymbol{U}$ as a linear combination over all the vibrational modes (which form a complete orthogonal basis set),[29]

$$\boldsymbol{U}(x,y,z,t) = \sum_n \alpha_n \boldsymbol{u}_n(x,y,z) \exp(-i\omega_n t) \tag{1}$$

where the subscript n refers to the nth mode, $\boldsymbol{u}_n(x,y,z)$ is the spatial displacement vector of mode n, ω_n are the radial resonant frequencies, and α_n are the corresponding Fourier coefficients. The vibrational modes are normalized so that $\int_V |\boldsymbol{u}_n|^2 \, dV = 1$. Given that displacements are infinitesimal within the framework of the theory of linear elasticity, the temporal response of the change in volume ΔV can be immediately calculated as[29]

$$\frac{\Delta V}{V} = \sum_n \gamma_n \exp(-i\omega_n t) \tag{2}$$

where ΔV is the change in volume, V is the initial volume of the box, and

$$\gamma_n = \frac{\alpha_n}{V} \int_S \hat{\boldsymbol{n}} \cdot \mathbf{u}_n \, dS \tag{3}$$

where $\hat{n}$ is the outward normal unit vector to the surface, and the integration is performed over all surfaces of the box.

The particle modes were calculated using finite element analysis, which requires the density, Young's modulus (E), Shear modulus (G), and Poisson's ratio (ν) for the different crystal directions in the particle. The specific formulas for $E_{[ij]}$, $G_{[ij]}$, and $\nu_{[ij]}$ are:[33]

$$E_{xx} = E_{yy} = E_{zz} = \frac{(C_{11} - C_{12})(C_{11} + 2C_{12})}{(C_{11} + C_{12})} \tag{4a}$$

$$G_{xy} = G_{yz} = G_{xz} = C_{44} \tag{4b}$$

$$\nu_{xy} = \nu_{yz} = \nu_{xz} = \frac{C_{12}}{C_{11} + C_{12}} \tag{4c}$$

where the C_{ij} are elastic constants of the material of the particle. The values used were those for a gold−silver alloy with an 3:1 Au−Ag atomic ratio, specifically: $C_{11} = 166.2$ GPa, $C_{12} = 132.4$ GPa, and $C_{44} = 48.4$ GPa, with the density $\rho = 17.1$ g/cm^3.[34] These values are appropriate for the majority of the samples used in these experiments. Note that using elastic constants for a Au−Ag atomic ratio of 2:1 (the lower limit for the samples in these experiments) does not significantly change the results.

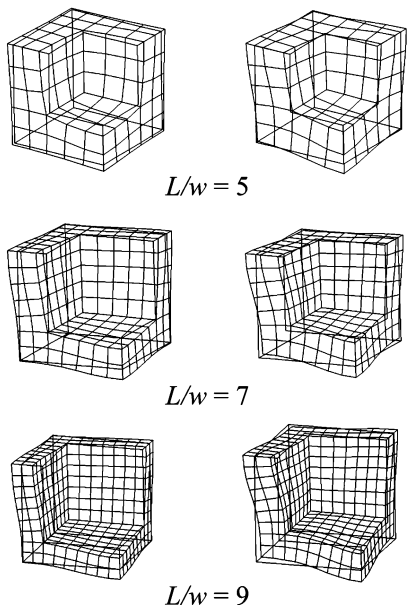

Figure 3. Shapes of the vibrational modes excited by volume expansion determined by finite element calculations (only $^1/_8$ of the box is shown). The mode shapes and their eigenfrequencies depend on the ratio of the edge length to wall thickness (L/w). The calculations pick out two modes; the lower frequency mode is given on the left.

The numerical analysis predicts that two main modes are excited by laser-induced heating. The eigenfrequencies and exact form of these modes depend on the ratio of the edge length to the wall thickness (L/w) of the box. The shapes of these two modes for different values of L/w are presented in Figure 3. The modes clearly correspond to breathing vibrations of the box. Figure 4 shows a plot of the normalized frequency $\bar{\omega} = \omega L\sqrt{\rho/E}$ determined from the theoretical analysis versus L/w. The size of the symbols in Figure 4 represents the relative value of γ_n for the mode (that is, the relative contribution of the mode to the change in volume). These results show that, at values of $L/w < 5$, the response of the particle should be dominated by the lower frequency of the two modes. In contrast, for $L/w > 6$, the higher frequency mode is expected to be dominant.

The reduced frequencies calculated from the experimental data are also plotted in Figure 4 as the square symbols (the bulk values of ρ and E were used to calculate the reduced frequencies). The samples in our experiments have values of $L/w > 7$, and the experimental reduced frequencies are close to the calculated values for the higher frequency mode. Thus, the experimental results are in good agreement with the predictions of the numerical calculations. The average difference between the experimental and calculated frequen-

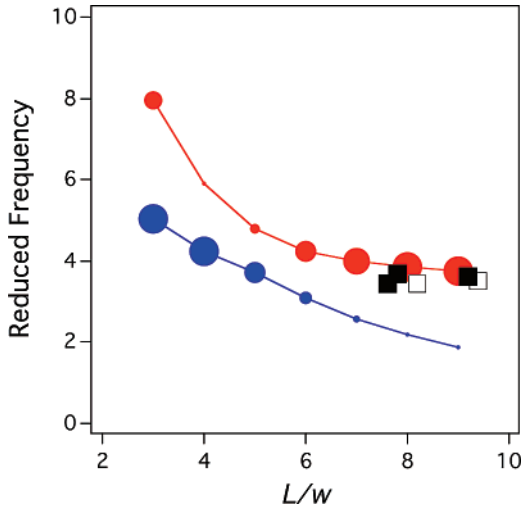

Figure 4. Calculated and measured reduced frequencies ($\bar{\omega} = \omega L\sqrt{\rho/E}$) for the different samples plotted as a function of L/w. The size of the symbols for the calculations (circles) represents the relative contribution of the mode to the volume change of the box. The square symbols represent the experimental reduced frequencies for the nanoboxes (filled symbols) and nanocages (open symbols). The error bars for the experimental reduced frequency are contained within the symbol.

cies is ~7% and shows no trend with L/w or whether the sample corresponds to nanocages or nanoboxes.

This deviation is slightly larger than the estimated uncertainties in the experiments and may indicate that the elastic constants of the nanoboxes and nanocages are smaller than the corresponding bulk material. However, there are two experimental artifacts that need to be taken into account in making a quantitative comparison between the measured elastic constants of the particles and the bulk values.[26] First, there is a moderate amount of lattice heating in our experiments (typically a few hundred Kelvin), which can lead to a reduction in the effective elastic moduli of the particles.[35] Second, because the optical absorption of the particles is proportional to volume,[13] the transient absorption experiments preferentially detect the larger particles in the sample.[26] Both of these effects account for a few percent reduction in the measured value of Young's modulus in the experiments.[26] Thus, the elastic constants of the nanoboxes and nanocages determined from these measurements are essentially within experimental error of the bulk values. This is in contrast to our recent studies of nanorods, where a significant decrease in the measured value of Young's modulus for the rods was observed.[26] However, it is consistent with studies of spherical particles[24,25] and with recent results for triangles[28] and cubes.[29]

It is important to note that, for particles with $L/w > 7$, the reduced frequency $\bar{\omega} = \omega L\sqrt{\rho/E}$ for the higher frequency mode does not depend strongly on L/w, see Figure 4. This is why the measured periods for the different samples scale with edge length in the same way, as shown by the inset in Figure 2. The line in this figure was generated using the average calculated value of $\bar{\omega}$ for the higher frequency mode for boxes with $L/w > 7$. Specifically, the period is given by $T = (2\pi/\langle\bar{\omega}\rangle)L\sqrt{\rho/E}$, where $\langle\bar{\omega}\rangle = 3.79$.

Guillon and co-workers recently reported time-resolved spectroscopy measurements of coherently excited vibrational modes in metal nanoshells.[36] The vibrational periods were on the order of 40 ps and scaled linearly with particle size, similar to the results obtained in the present study. The authors also presented analytic expressions for the vibrational frequencies and damping times in terms of the particle dimensions and the transverse and longitudinal speeds of sound.[36] Analytic expressions are desirable because they provide a direct link between the experimental measurements and the elastic constants.[22,24−26] The theory correctly predicted the trends in the experimental results. However, the experimental and calculated periods differed by approximately a factor of 2.[36] Thus, it is not possible to derive quantitative information about the elastic constants of the particles from these measurements.

In summary, this paper presents a combined experimental time-resolved spectroscopy and finite element analysis study of the vibrational response of Au−Ag nanoboxes and nanocages to laser-induced heating. Very good agreement was obtained between the experiments and calculations. Specifically, the calculations predict that two modes should be excited by laser-induced heating, with the lower frequency mode being dominant at values of the edge length to wall thickness ratio $L/w < 5$, and the higher frequency mode being dominant at $L/w > 6$. The particles in this study had values of $L/w > 7$, and the measured vibrational frequencies were in good agreement with the higher frequency mode, as predicted by the numerical calculations. This is not a trivial result: visually the two modes picked out by the numerical calculations are very similar (see Figure 3) and, in general, the lower frequency mode dominates the response in time-resolved studies of nanoparticle vibrations.[30] Thus, the fact that the numerical calculations correctly predict that the high-frequency mode is excited shows the power of this analysis. The good match between the experimental and calculated frequencies implies that the elastic constants of these hollow particles are essentially the same as the bulk material. Taken together, these results emphasize the importance of numerical modeling in describing the response of complex-shaped particles to laser-induced heating.[28,29]

Acknowledgment. Y.X. acknowledges the support of NIH (Director's Pioneer Award) and NSF (DMR-0451788). G.V.H. acknowledges the support of the NSF and the Petroleum Research Fund, administered by the American Chemical Society. The work in Australia was supported by the Particulate Fluids Processing Centre and the Australian Research Council grants scheme.

References

(1) See articles in the special issue on Anisotropic Nanomaterials in *J. Mater. Chem.* **2006**, *16*.
(2) Murphy, C. J.; San, T. K.; Gole, A. M.; Orendorff, C. J.; Gao, J. X.; Gou, L.; Hunyadi, S. E.; Li, T. *J. Phys. Chem. B* **2005**, *109*, 13857−13870.
(3) Perez-Juste, J.; Pastoriza-Santos, I.; Liz-Marzan, L. M.; Mulvaney, P. *Coord. Chem. Rev.* **2005**, *249*, 1870−1901.
(4) Jin, R. C.; Cao, Y. W.; Mirkin, C. A.; Kelly, K. L.; Schatz, G. C.; Zheng, J. G. *Science* **2001**, *294*, 1901−1903.
(5) Callegari, A.; Tonti, D.; Chergui, M. *Nano Lett.* **2003**, *3*, 1565−1568.

(6) Sun, Y. G.; Xia, Y. N. *Science* **2002**, *298*, 2176−2179.
(7) Manna, L.; Milliron, D. J.; Meisel, A.; Scher, E. C.; Alivisatos, A. P. *Nat. Mater.* **2003**, *2*, 382−385.
(8) Kuno, M.; Ahmad, O.; Protasenko, V.; Bacinello, D.; Kosel, T. H. *Chem. Mater.* **2006**, *18*, 5722−5732.
(9) Haes, A. J.; Van Duyne, R. P. *Anal. Bioanal. Chem.* **2004**, *379*, 920−930.
(10) Schultz, S.; Smith, D. R.; Mock, J. J.; Schultz, D. A. *Proc. Natl. Acad. Sci. U.S.A.* **2000**, *97*, 996−1001.
(11) West, J. L.; Halas, N. J. *Annu. Rev. Biomed. Eng.* **2003**, *5*, 285−292.
(12) Huang, X. H.; Jain, P. K.; El-Sayed, I. H.; El-Sayed, M. A. *Photochem. Photobiol.* **2006**, *82*, 412−417.
(13) Kreibig, U.; Vollmer, M. *Optical Properties of Metal Clusters*, Springer: Berlin, 1995.
(14) Kelly, K. L.; Coronado, E.; Zhao, L. L.; Schatz, G. C. *J. Phys. Chem. B* **2003**, *107*, 668−677.
(15) Sonnichsen, C.; Franzl, T.; Wilk, T.; von Plessen, G.; Feldmann, J.; Wilson, O.; Mulvaney, P. *Phys. Rev. Lett.* **2002**, *88*, 077402.
(16) Mock, J. J.; Barbic, M.; Smith, D. R.; Schultz, D. A.; Schultz, S. *J. Chem. Phys.* **2002**, *116*, 6755−6759.
(17) Novo, C.; Gomez, D.; Perez-Juste, J.; Zhang, Z. Y.; Petrova, H.; Reismann, M.; Mulvaney, P.; Hartland, G. V. *Phys. Chem. Chem. Phys.* **2006**, *8*, 3540−3546.
(18) Berciaud, S.; Cognet, L.; Tamarat, P.; Lounis, B. *Nano Lett.* **2005**, *5*, 515−518.
(19) Sherry, L. J.; Jin, R.; Mirkin, C. A.; Schatz, G. C.; Van Duyne, R. P. *Nano Lett.* **2006**, *6*, 2060−2065.
(20) Voisin, C.; Christofilos, D.; Loukakos, P. A.; Del Fatti, N.; Vallee, F.; Lerme, J.; Gaudry, M.; Cottancin, E.; Pellarin, M.; Broyer, M. *Phys. Rev. B* **2004**, *69*, 195416.
(21) Arbouet, A.; Voisin, C.; Christofilos, D.; Langot, P.; Del Fatti, N.; Vallee, F.; Lerme, J.; Celep, G.; Cottancin, E.; Gaudry, M.; Pellarin, M.; Broyer, M.; Maillard, M.; Pileni, M. P.; Treguer, M. *Phys. Rev. Lett.* **2003**, *90*, 177401.
(22) Hartland, G. V. *Phys. Chem. Chem. Phys.* **2004**, *6*, 5263−5274.
(23) Hu, M.; Petrova, H.; Chen, J. Y.; McLellan, J. M.; Siekkinen, A. R.; Marquez, M.; Li, X. D.; Xia, Y. N.; Hartland, G. V. *J. Phys. Chem. B* **2006**, *110*, 1520−1524.
(24) Voisin, C.; Del Fatti, N.; Christofilos, D.; Vallee, F. *J. Phys. Chem. B* **2001**, *105*, 2264−2280.
(25) Hartland, G. V. *Annu. Rev. Phys. Chem.* **2006**, *57*, 403−430.
(26) Petrova, H.; Perez-Juste, J.; Zhang, Z. Y.; Zhang, J.; Kosel, T. H.; Hartland, G. V. *J. Mater. Chem.* **2006**, *16*, 3957−3963.
(27) Sader, J. E.; Hartland. G. V.; Mulvaney, P. *J. Phys. Chem. B* **2002**, *106*, 1399−1402.
(28) Bonacina, L.; Callegari, A.; Bonati, C.; van Mourik, F.; Chergui, M. *Nano Lett.* **2006**, *6*, 7−10.
(29) Petrova, H.; Lin, C. H.; de Liejer, S.; Hu, M.; McLellan, J. M.; Siekkinen, A. R.; Wiley, B. J.; Marquez, M.; Xia, Y.; Sader, J. E.; Hartland, G. V. *J. Chem. Phys*. **2007**, *126*, 094709.
(30) Hu, M.; Wang, X.; Hartland, G. V.; Mulvaney, P.; Perez-Juste, J.; Sader, J. E. *J. Am. Chem. Soc*. **2003**, *125*, 14925−14933.
(31) Chen, J. Y.; Wiley, B.; Li, Z. Y.; Campbell, D.; Saeki, F.; Cang, H.; Au, L.; Lee, J.; Li, X. D.; Xia, Y. N. *Adv. Mater.* **2005**, *17*, 2255−2261.
(32) Hodak, J. H.; Martini, I.; Hartland, G. V. *J. Phys. Chem. B* **1998**, *102*, 6958−6967.
(33) Landau, L. D.; Lifshitz, E. M. *Theory of Elasticity*, 2nd ed.; Pergamon Press; Oxford, 1970.
(34) Simmons, G.; Wang, H. *Single Crystal Elastic Constants and Calculated Aggregate Properties: A Handbook*, The MIT Press: Cambridge, 1971.
(35) Petrova, H.; Perez-Juste, J.; Pastoriza-Santos, I.; Hartland, G. V.; Liz-Marzan, L. M.; Mulvaney, P. *Phys. Chem. Chem. Phys.* **2006**, *8*, 814−821.
(36) Guillon, C.; Langot, P.; Del Fatti, N.; Vallée, F.; Kirakosyan, A. S.; Shahbazyan, T. V.; Cardinal, T.; Treguer, M. *Nano Lett.* **2007**, *7*, 138−142.

NL0702766